

# Effect of grain boundary microstructure on fatigue crack propagation in austenitic stainless steel

Shigeaki Kobayashi · Manabu Nakamura ·  
Sadahiro Tsurekawa · Tadao Watanabe

Received: 23 August 2010 / Accepted: 30 December 2010 / Published online: 15 January 2011  
© Springer Science+Business Media, LLC 2011

**Abstract** The effect of grain boundary microstructure on fatigue crack propagation in austenitic stainless steel was investigated in order to control fatigue crack propagation. The fraction of low- $\Sigma$  coincidence boundaries in specimens was controlled by thermomechanical processing. The specimen with the higher fraction of low- $\Sigma$  boundaries (73%) showed the lower propagation rate of fatigue crack than the specimen with the lower fraction of low- $\Sigma$  boundaries (53%). The ratio of intergranular fracture segments to the total crack length was lower for the specimen with the higher fraction of low- $\Sigma$  boundaries. Moreover, the roles of grain boundaries in the fatigue crack propagation were investigated in connection with grain boundary microstructure, i.e., the character distribution and geometrical configuration of grain boundaries. It is evidenced that the approach to grain boundary engineering is applicable to controlling fatigue crack propagation in austenitic stainless steel.

## Introduction

Grain boundary engineering (GBE) has been extensively applied to the improvement in bulk properties and development of high performance in polycrystalline materials [1, 2] by controlling various types of brittleness due to corrosion [3–5], creep [6], and segregation [7]. Recently, GBE was successfully applied to develop high-performance structural materials like austenitic stainless steels. Lo et al. have overviewed the recent development of stainless steel from various points of view including GBE [8]. For the materials with a low stacking fault energy, GBE was achieved by introducing a high fraction of  $\Sigma 3$ -related ( $\Sigma = 3^n$ ) coincidence boundaries caused by multiple-twinning. However, it has been found that the coherent twin boundaries, that is  $\{111\}/\Sigma 3$  boundaries, can be preferential sites for crack nucleation in fatigue fracture of fcc metals and alloys [9, 10], although the  $\{111\}/\Sigma 3$  boundaries are well-known to possess the lowest boundary energy [11] and the highest fracture strength under static stress condition [12, 13]. This preferential fatigue cracking of the  $\{111\}/\Sigma 3$  boundaries is ascribed to the stress concentration as the result of the significant interaction between the  $\{111\}/\Sigma 3$  boundary and localized crystal slip during fatigue deformation [10]. According to our recent investigation of fatigue fracture in a coarse-grained polycrystalline pure aluminum [14], low-angle and low- $\Sigma$  coincidence boundaries possess a higher resistance to fatigue crack nucleation than high-angle random boundaries. At low- $\Sigma$  coincidence boundaries, fatigue cracks were only observed when the trace of these boundaries was parallel to persistent slip bands on the specimen surface. Accordingly, it is important to study the effects of grain boundary character and geometrical configuration of low- $\Sigma$  coincidence boundaries on the crack nucleation and

S. Kobayashi (✉) · M. Nakamura  
Department of Mechanical Engineering, Faculty of Engineering,  
Ashikaga Institute of Technology, Omae-cho 268-1, Ashikaga,  
Tochigi 326-8558, Japan  
e-mail: skoba@ashitech.ac.jp

S. Tsurekawa  
Department of Materials Science and Engineering, Graduate  
School of Science and Technology, Kumamoto University,  
Kumamoto 860-8555, Japan

Present Address:  
T. Watanabe  
Key Laboratory for Anisotropy and Texture of Materials,  
Northeastern University, Shenyang 110004, China

T. Watanabe  
Tohoku University, Sendai, Japan

propagation in connection with preferential roles of the  $\{111\}/\Sigma 3$  boundaries in fatigue fracture.

Kaneko et al. have studied fatigue crack propagation in copper bicrystals with near  $\{111\}/\Sigma 3$  boundaries [15], and revealed that the propagation of fatigue cracks is strongly affected by the deviation from the exact misorientation angle for the  $\{111\}/\Sigma 3$  boundary. When the deviation of misorientation angle is  $<3^\circ$ , the fatigue cracks never propagate along the  $\Sigma 3$  boundaries. The ratio of intergranular cracking increased in the specimens having the deviation angle ranging from  $3^\circ$  to  $5^\circ$ . On the other hand, when the deviation angle is more than  $9^\circ$ , fatigue cracks can propagate predominantly in the grain interior. Therefore, from the viewpoint of structure-dependent crack propagation,  $\{111\}/\Sigma 3$  boundary does not necessarily degrade fatigue fracture properties. Thus, the fatigue crack propagation can be controlled by optimization of grain boundary microstructure in polycrystalline materials. However, only a little study has been performed so far on the GBE for improvement in fatigue property in polycrystalline materials [16–18]. Lehockey et al. have reported that the fatigue life of Ni-based alloy was improved by increasing the fraction of low- $\Sigma$  boundaries [16]. In contrast, Gao et al. have reported that there is little influence of the fraction of low- $\Sigma$  boundaries on the propagation rate of fatigue fracture at an ambient temperature, while the resistance to crack growth at elevated temperatures was evidently improved by introduction of a higher fraction of low- $\Sigma$  boundaries [17]. There is a large difference in the previous results on the effect of grain boundary microstructure on fatigue properties. A further investigation is necessary to establish the GBE for improvement in fatigue fracture property.

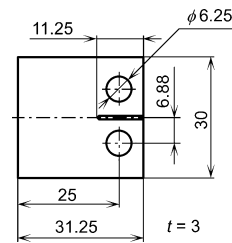
In this work, the applicability of GBE for the control of fatigue crack propagation in SUS304 austenitic stainless steel was investigated by using the specimens with different grain boundary microstructures produced by thermomechanical processing. The effects of grain boundary microstructure, particularly the grain boundary character distribution (GBCD) and geometrical configuration of grain boundaries, on fatigue crack propagation was investigated.

## Experimental procedure

### Specimen preparation

Fully pre-annealed SUS304 stainless steel sheets were subjected to cold rolling to 5, 10, and 20% in strain, and then these cold-rolled sheets were subsequently annealed at 1,273 K for 3.6 ks, in order to obtain different grain boundary microstructures, with making reference to the previous work by others on the control of grain boundary

**Fig. 1** The shape and dimensions of the specimens for compact tension fracture test



microstructure by thermomechanical processing in the stainless steel [3–5]. The specimens for compact tension (CT) fracture test were cut from the annealed sheets with a spark machine. The dimensions of the specimen were 30-mm wide and 3.0-mm thick as shown in Fig. 1. The surface of the specimens was mechanically polished using 320–1500 grade emery papers, and then electrolytically polished to remove residual strain near surface layer in an electrolytic solution of acetic acid and perchloric acid of 77:23 in volume fraction at a current density of  $0.15 \text{ A/cm}^2$  at 280 K for 60 s.

### Characterization of grain boundary microstructure

The grain boundary microstructure was determined by field emission-scanning electron microscopy (FE-SEM)/electron backscattered diffraction (EBSD)/orientation imaging microscopy (OIM). The SEM/EBSD/OIM observations were performed on Hitachi S-4200 FE-SEM equipped with TSL's OIM. In this work, the grain boundary character was described by  $\Sigma$ -value with  $1 \leq \Sigma \leq 29$ , which were defined as low- $\Sigma$  coincidence site lattice (CSL) boundaries within the maximum allowable angular deviation from the exact CSL orientation according to the Brandon's criterion,  $\Delta\theta = 15/\Sigma^{1/2}$  [19], as widely applied so far. Moreover, the grain boundary microstructure should be more precisely characterized in polycrystalline material, by determining not only GBCD but also other geometrical parameters such as the grain boundary connectivity [2, 20] and grain boundary plane-orientation distribution [21]. Up to now there have been extensive experimental observations that CSL boundaries with  $\Sigma$ -value  $<29$  show special properties which high-energy random boundaries never show [8, 22, 23], under our present recognition that the grain boundary energy is not simply and uniquely determined by special misorientation relationships defined by the  $\Sigma$ -value, and moreover CSL boundaries should be classified into three groups depending on  $\Sigma$ -value for fcc crystals, but not for bcc crystals which the grain boundary energy simply depends on the  $\Sigma$ -value, as clearly pointed out by Smith [24]. In this work, the fraction of low- $\Sigma$  CSL boundaries was determined by the total length of segments of low- $\Sigma$  CSL boundaries based on OIM analyses.

## Fatigue crack propagation tests

Fatigue crack propagation tests were carried out by using a servo-hydraulic machine (Shimadzu Servopulser) in air at room temperature. Sinusoidal loading on different levels were applied at the load ratio of  $R = 0.1$  and at the frequency of 5 Hz. Fatigue tests were carried out on the stress intensity factors,  $\Delta K$ , ranging from 50 to 90 MPa m $^{1/2}$ , which is given by ASTM standard E-647 [25]. The length of fatigue cracks was measured by optical microscope when the specimen was cyclically deformed to predetermined number of cycles of loading. The propagation path of fatigue cracks was evaluated in connection with the grain boundary microstructures.

## Results and discussion

### Control of grain boundary microstructure by thermomechanical processing

Figure 2a–c shows the typical OIM micrographs with the data of the average grain size and the inverse pole figure for the three specimens differently produced by thermomechanical processing. In these OIM micrographs, the types of grain boundaries are shown in different colors corresponding to those color bars indicated on the right-hand side. For example, low-angle ( $2^\circ$ – $15^\circ$ ),  $\Sigma 3$  and random boundaries are shown by red, green, and black lines, respectively. The average grain sizes of the specimens cold-rolled to 5, 10, and 20% were 23, 21, and 19  $\mu\text{m}$ , respectively. The average grain size was systematically changed with increasing the reduction ratio of cold rolling before annealing. The surface orientation of specimens seems randomly distributing irrespective of the reduction ratio of cold rolling, as shown in the inverse pole figures. Moreover, a large number of  $\Sigma 3$  boundaries, which resulted from the formation of annealing twins, were observed in all the specimens. In this work, these  $\{111\}/\Sigma 3$  coherent annealing twin boundaries hereafter denoted as  $\Sigma 3$

**Fig. 2** OIM micrographs with the data of the average grain size, the inverse pole figure for specimens subjected to cold rolling to **a** 5%, **b** 10%, and **c** 20% and subsequent annealing (Color figure online)

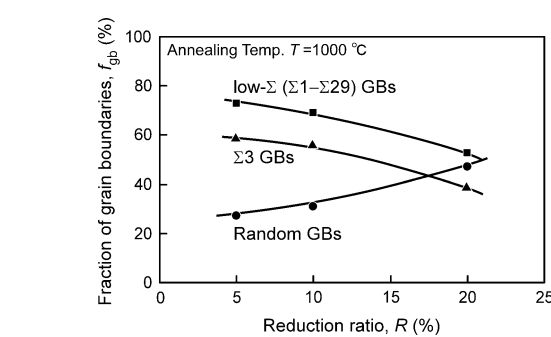
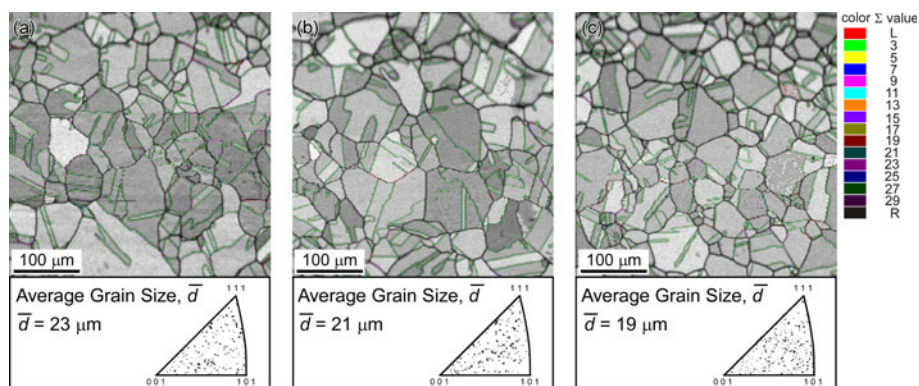


**Fig. 3** The fraction of grain boundaries with different characters as a function of the reduction ratio of cold rolling

boundaries, since the fraction of incoherent  $\Sigma 3$  boundaries was very small.

Figure 3 shows the fraction of grain boundaries with distinct characters as a function of the reduction ratio of cold rolling. The fraction of low- $\Sigma$  and  $\Sigma 3$  boundaries monotonously increased with decreasing reduction ratio of cold rolling before annealing. In contrast, the fraction of random boundaries decreased with decreasing the reduction ratio. A high fraction of low- $\Sigma$  boundaries (73%) including  $\Sigma 3$  boundaries (58%) was obtained for the specimen subjected to 5% cold rolling and subsequent annealing. On the other hand, the specimen subjected to 20% cold rolling and subsequent annealing possessed the lowest fraction of low- $\Sigma$  boundaries (53%) including  $\Sigma 3$  boundaries (47%). The dependence of the fraction of low- $\Sigma$  boundaries on the reduction ratio of cold rolling was in good agreement with the result from recent work by Michiuchi et al. on the GBCD in SUS316 austenitic stainless steel [5].

### Effect of GBCD on the propagation rate of fatigue cracks

Crack propagation was observed during fatigue tests for the two types of specimens having different fractions of low- $\Sigma$  boundaries: Type A (73%) and Type B (53%) to examine

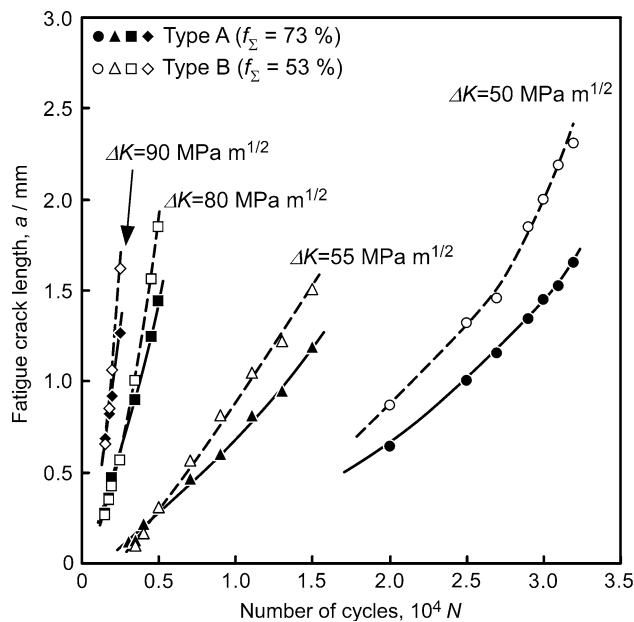


**Fig. 4** Relationship between the total length of fatigue cracks and the number of cycles on different levels of the stress intensity, for the Type A and Type B specimens

the effect of GBCD on fatigue crack propagation. The Type A and Type B specimens showed almost the same tensile properties irrespective of the GBCDs. The yield stress of these specimens was 224 MPa. Figure 4 shows the relationship between the length of fatigue cracks and the number of cycles for the Type A and the Type B specimens. This is obtained from the fatigue crack propagation tests for four different stress intensity factors,  $\Delta K$ . The length of fatigue cracks were strongly affected by the GBCD in the specimens. The length of fatigue crack in the Type A specimen with a higher fraction of low- $\Sigma$  boundaries ( $f_{\Sigma} = 73\%$ ) was by 20–30% shorter than that in the Type B specimen ( $f_{\Sigma} = 53\%$ ) at all the value of  $\Delta K$  in this work. Figure 5 shows the relationship between the propagation rate of fatigue cracks and the stress intensity factor for the Type A and the Type B specimens. The propagation rate of fatigue cracks in the Type A specimen was lower than that in the Type B specimen. Therefore, it is evidenced that the fatigue crack propagation in the SUS304 austenitic stainless steel is definitely controlled by GBCD.

According to recent work by Gao et al. on fatigue fracture in nickel-based superalloy, the propagation rate of fatigue crack at an ambient temperature was less influenced by GBCDs [17]. The observed smaller influence of GBCD on fatigue crack propagation was explained by the predominant contribution of transgranular fracture mode. Accordingly, we observed the paths of crack propagation in fatigue fracture in SUS304 austenitic stainless steel to reveal GBCD-dependent fatigue crack propagation.

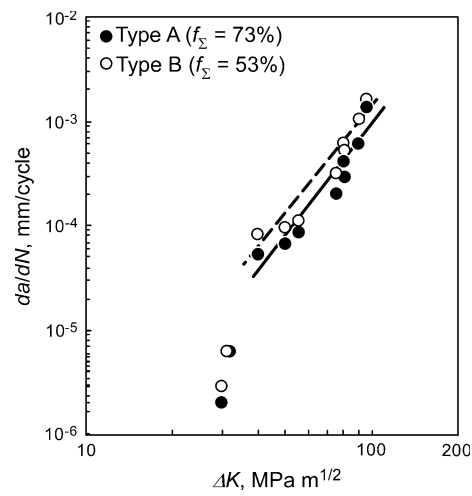


**Fig. 5** Relationship between the propagation rate of fatigue cracks and the level of the stress intensity  $\Delta K$ , for Type A and Type B specimens

#### Roles of grain boundaries in propagation process of fatigue cracks

Figure 6a and b shows the path of fatigue crack propagation in Type A and Type B specimens which cyclically deformed at the stress intensity factor of  $50 \text{ MPa m}^{1/2}$ , respectively. The white lines drawn along the fatigue crack are the paths where fatigue crack propagates along the grain boundaries. It was found that the fatigue cracks propagated predominantly in the manner of transgranular fracture rather than intergranular fracture in the two types of studied specimens. Particularly, the ratio of the segments of intergranular fracture to the total crack length for the Type A specimen was smaller than that for the Type B specimen. Table 1 shows the propagation rate of fatigue crack, the fraction of transgranular and intergranular fracture to the overall fracture path for the Type A and the Type B specimens cyclically deformed at different stress intensity factors. The contributions of intergranular fracture to the total crack length,  $F_i$ , are 7–20% for the Type A, and 18–31% for the Type B specimens. Conversely, the contribution of transgranular fracture to the total crack length,  $F_t$ , is much larger for the Type A specimen (with a higher fraction of low- $\Sigma$  boundaries) than for the Type B specimen (with a lower fraction of low- $\Sigma$  boundaries). This result demonstrates that the observed fatigue fracture occurred dominantly by crack propagation involving mainly transgranular fracture at all values of  $\Delta K$ . The difference in the ratio of intergranular fracture to the total crack length may reflect the difference between the crack propagation rates of the Type A and the Type B specimens. Surprisingly, the difference between  $F_t$  (or  $F_i$ ) for the Type A specimen and that of the Type B specimen seems reasonably corresponding to the difference in the fraction of

**Fig. 6** Optical micrographs of fatigue cracks in Type A and Type B specimens cyclically deformed at the stress intensity level of  $50 \text{ MPa m}^{1/2}$

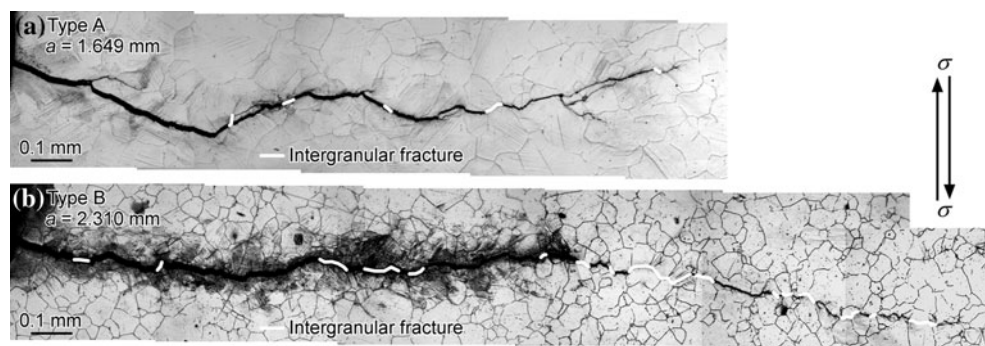


**Table 1** The propagation rate of fatigue crack, the fraction of transgranular or intergranular fracture to the overall fracture path for Type A and Type B specimens cyclically deformed on different levels of the stress intensity,  $\Delta K$

| Specimen | $\Delta K (\text{MPa m}^{1/2})$ | $da/dN (\text{mm/cycle})$ | $F_t (\%)$ | $F_i (\%)$ |
|----------|---------------------------------|---------------------------|------------|------------|
| Type A   | 50                              | $8 \times 10^{-5}$        | 93         | 7          |
|          | 55                              | $9 \times 10^{-5}$        | 90         | 10         |
|          | 80                              | $3 \times 10^{-4}$        | 90         | 10         |
|          | 90                              | $6 \times 10^{-4}$        | 80         | 20         |
| Type B   | 50                              | $9 \times 10^{-5}$        | 72         | 28         |
|          | 55                              | $1 \times 10^{-4}$        | 77         | 23         |
|          | 80                              | $5 \times 10^{-4}$        | 82         | 18         |
|          | 90                              | $1 \times 10^{-3}$        | 69         | 31         |

$F_t$  transgranular fracture,  $F_i$  intergranular fracture

low- $\Sigma$  boundaries, suggesting the role of strongest link of low- $\Sigma$  boundaries in fatigue crack propagation.

It is not so unreasonable to expect that if the ratio of intergranular fracture to the total crack length can be changed by the introduction of a higher fraction of low- $\Sigma$  boundaries, the propagation rate of fatigue cracks may be naturally affected as one of the present authors predicted in the original concept of the GBE [20]. Let us discuss this point in detail in the next section.

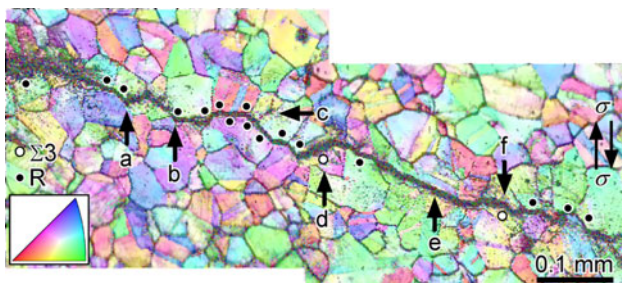
#### Effect of grain boundary character on the fatigue crack propagation

As shown in the previous section, the fatigue crack propagation in the austenitic stainless steel was found to be affected by the GBCD. From the viewpoint of GBE, it is important to quantitatively evaluate the effect of grain boundaries with different levels of intergranular fracture resistance on crack propagation. Vinogradov et al. [26] have studied the effect of the grain boundary character on fatigue crack propagation by using copper bicrystal specimens including  $\Sigma 9$  and random boundaries with the same geometry to the tensile-orientation axis. They found that fatigue fracture mode changes from transgranular fracture to intergranular or mixed fracture when the fatigue cracks

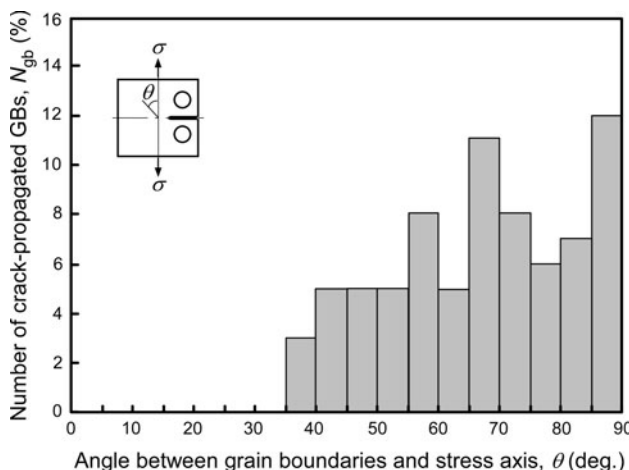
reach the random boundary, while the fatigue cracks were never observed along  $\Sigma 9$  boundary, suggesting a higher fracture resistance of  $\Sigma 9$  boundary in fatigue fracture. Until presently, there has been little work on the effect of the grain boundary character on fatigue crack propagation. The present work has revealed the effect of GBCD on fatigue crack propagation in polycrystalline specimens of stainless steel.

Figure 7 shows an OIM micrograph which shows the propagation path of fatigue crack in the Type B specimen cyclically deformed at the stress intensity factor of  $50 \text{ MPa m}^{1/2}$ . The OIM micrograph shows the geometrical shape and the arrangement of individual grains with different crystal orientations in a polycrystal specimen, indicated in distinct/gradient colors in the stereo-triangle on the left-bottom corner, in order to clarify the propagation path of fatigue crack. The fatigue crack was deflected depending on the direction of persistent slip bands in the adjacent grain when the surface orientation of adjacent grains was different.

$\Sigma 3$  and random boundaries lying along the main fatigue crack are marked by white and black dots, respectively. The fatigue crack does not necessarily propagate along random boundaries, and their propagation path sometimes changed from intergranular fracture to transgranular fracture as shown within a specific region indicated by arrows and letters a and b in Fig. 7. On the other hand, the fatigue cracks along  $\Sigma 3$  boundaries was observed only when the boundary trace on the specimen surface was coincident with the direction of fatigue crack propagation within the range indicated by letters d and f. In the region indicated by letter e, the fatigue crack was propagated grain interior parallel to  $\Sigma 3$  boundary. Moreover, the  $\Sigma 3$  boundary might inhibit fatigue crack propagation when the trace of  $\Sigma 3$  boundary was nearly parallel to the stress axis, as in the region c. From the present observations, it is suggested that the geometrical configuration of grain boundaries with respect to the stress axis, as well as grain boundary character, may play some key role in fatigue crack propagation in SUS304 austenitic stainless steel.



**Fig. 7** OIM micrograph showing the path of fatigue crack propagation in Type B specimen cyclically deformed at the stress intensity level of  $50 \text{ MPa m}^{1/2}$



**Fig. 8** The effect of the grain boundary inclination on fatigue crack propagation in austenitic stainless steel specimens

#### Effect of geometrical configuration of grain boundaries on fatigue crack propagation

The effects of geometrical configuration of grain boundaries on fatigue crack nucleation [27–31] and propagation [32, 33] has been investigated using bicrystalline and polycrystalline specimens of metals. Lim has shown that the fatigue crack propagation is accelerated if the grain boundary plane is aligned at a larger angle to the stress axis in a coarse-grained nickel [32]. Figure 8 shows the relationship between the number of grain boundaries which allowed fatigue crack to propagate and the angle between the grain boundary trace on the specimen surface and the stress axis. In this figure, the angles of  $0^\circ$  and  $90^\circ$  means that the grain boundary trace is parallel and perpendicular to the stress axis, respectively. It was found that fatigue cracks never propagate along grain boundaries when the angles between the boundary trace and the stress axis is  $<35^\circ$ . On the other hand, the fatigue cracks propagate along grain boundaries when the angle between the grain boundary trace direction and the stress axis is larger than

$35^\circ$ . Particularly, the grain boundaries with the angles ranging from  $55^\circ$  to  $90^\circ$  to the stress axis can be the preferential paths for fatigue crack propagation. Thus, the crack propagation path during fatigue in austenitic stainless steel is markedly affected not only by the grain boundary character, but also by the geometrical configuration of the grain boundary plane to the stress axis. These results are consistent with the results obtained by Lim [32].

From the results in the present work, it is concluded that the propagation of fatigue crack in polycrystalline austenitic stainless steel can be controlled by manipulating the GBCD and geometrical configuration of grain boundaries, as predicted by the concept of GBE.

#### Conclusions

The effect of the grain boundary microstructure on fatigue crack propagation was investigated for the specimens prepared by thermomechanical processing in SUS304 austenitic stainless steel, in order to prove the applicability of GBE for controlling fatigue crack propagation. The main conclusions are as follows:

1. Thermomechanical processing based on cold rolling and subsequent annealing could produce a high fraction of low- $\Sigma$  boundaries (73%) including  $\Sigma 3$  boundaries (58%) for the specimen subjected to 5% cold rolling and subsequent annealing. On the other hand, specimen subjected to 20% cold rolling and subsequent annealing showed a lower fraction of low- $\Sigma$  boundaries (53%) including  $\Sigma 3$  boundaries (39%).
2. The propagation rate of fatigue crack was lower for the specimen with a high fraction of low- $\Sigma$  boundaries than for the specimen with a low fraction of low- $\Sigma$  boundaries.
3. The contribution of intergranular fracture to the total crack length was lower for the specimen with a high fraction of low- $\Sigma$  boundaries than for the specimen with a low fraction of low- $\Sigma$  boundaries. Intergranular fatigue crack was found to preferentially propagate along random boundaries.
4. Fatigue cracks never propagate along such grain boundaries whose trace direction was aligned by the angles smaller than  $35^\circ$  from the stress axis, while the grain boundaries with those angles larger than  $55^\circ$  are likely to be the paths for fatigue crack propagation.

**Acknowledgements** The present work was financially supported by the Grant-in-Aid for Young Scientists (B) (21760560) of the Ministry of Education, Culture, Sports, Science and Technology, Japan and by a project on Collaborative Research at the Collaborative Research Center of Ashikaga Institute of Technology. T.W. acknowledges support by Northeastern University, Shenyang, China in collaboration

with Prof. L. Zuo and Prof. X. Zhao through the 111 project (Grant No. 1307015).

## References

1. Palumbo G, Leockey EM, Lin P (1998) JOM 50:40
2. Watanabe T, Tsurekawa S (1999) Acta Mater 47:4171
3. Shimada M, Kokawa H, Wang ZJ, Sato YS, Karibe I (2002) Acta Metall 50:2331
4. Tsurekawa S, Nakamichi S, Watanabe T (2006) Acta Mater 54:3617
5. Michiuchi M, Kokawa H, Wang ZJ, Sato YS, Sakai K (2006) Acta Mater 54:5179
6. Thaveeprungsripon V, Was GS (1997) Metall Mater Trans A28:2101
7. Kobayashi S, Tsurekawa S, Watanabe T, Palumbo G (2010) Scr Mater 62:294
8. Lo KH, Shek CH, Lai JKL (2009) Mater Sci Eng R65:39 chap 9
9. Neumann P, Tönnessen A (1987) In: Proceedings of the third international conference on fatigue and fatigue thresholds (fatigue '87), Virginia, June 1987, p 3
10. Heinz A, Neumann P (1990) Acta Metall Mater 38:1933
11. Sutton A, Balluffi RW (1987) Acta Metall 35:2177
12. Kargol JA, Albright DL (1977) Metall Trans 8A:27
13. Otsuki A, Mizuno M (1986) In: Grain boundary structure and related phenomena, Proc. of JIMIS-4, suppl. to trans. Japan Institute of Metals, vol 27, pp 789–796
14. Kobayashi S, Inomata T, Kobayashi H, Tsurekawa S, Watanabe T (2008) J Mater Sci 43:3792. doi:[10.1007/s10853-007-2236-z](https://doi.org/10.1007/s10853-007-2236-z)
15. Kaneko Y, Kitagawa K, Hashimoto S (1999) Interface Sci 7:147
16. Leockey EM, Palumbo G, Lin P (1998) Metall Mater Trans A29:3069
17. Gao Y, Kumar M, Nalla RK, Ritchie RO (2005) Metall Mater Trans A36:3325
18. Gao Y, Stölken JS, Kumar M, Ritchie RO (2007) Acta Mater 55:3155
19. Brandon DG (1966) Acta Metall 14:1479
20. Watanabe T (1984) Res Mech 11:47
21. Rohrer GS, Saylor DM, Dasher BE, Adams BL, Rollet AD, Wymblatt P (2004) Z Metall 95:197
22. Watanabe T (1985) J Phys 46:C4-555
23. Yamaura S, Igarashi Y, Tsurekawa S, Watanabe T (1999) Acta Mater 47:1163
24. Smith DA (1974) Scr Metall 8:1197
25. Annual Book of ASTM Standards (2001) E647. ASTM, West Conshohocken
26. Vinogradov A, Hashimoto S, Miura S (1995) Scr Metall Mater 32:427
27. Kim WH, Laird C (1978) Acta Metall 26:777
28. Kim WH, Laird C (1978) Acta Metall 26:789
29. Mima G, Inoko F, Atagi K (1980) Trans Jpn Inst Met 21:89
30. Inoko F, Atagi K, Mima G (1982) Trans Jpn Inst Met 23:161
31. Hashimoto S, Ikehata H, Kato A, Kato H, Kaneko Y (1999) Interface Sci 7:159
32. Lim LC (1987) Acta Metall 35:1653
33. Hashimoto S, Kaneko Y (1999) Mater Sci Forum 294–296:685